Supplementary Information (SI) for ChemComm.

Methanesulfonic acid (MSA) and SO_3 formation from the addition channel of atmospheric dimethyl sulfide oxidation

Torsten Berndt

Contents

1. Experimental approach and product analysis

The experiments were carried out in a laminar flow tube (LFT), operating at 1 bar of air at a temperature of 295 ± 0.5 K and a relative humidity of < 0.1 %. A humidity sensor (Hygrosense HYTE) continuously controlled the relative humidity of the reaction gas. The total flow was set at 30 L min^{-1} (STP) resulting in a reaction time of 32 s, as experimentally determined using a "chemical clock". More detailed information on the experimental set-up is given elsewhwere.[1,2]

Photolysis of isopropyl nitrite (IPN) by 24 36 W BLB lamps, emitting in the range 350 - 400 nm, was chosen for OH radical production. IPN photolysis forms i-C_3H_7O radicals and NO followed by the rapid reaction of i-C_3H_7O radicals with O_2 generating HO_2 radicals. Finally, the OH radial formation proceeds via the reaction $NO + HO_2 \rightarrow OH + NO_2$.[3]

For dosing dimethyl sulfoxide ($CH_3S(O)CH_3$), a vial containing this substance was directly connected to the main air stream just before entering the LFT. Diffusion of $CH_3S(O)CH_3$ from the vial was sufficient to get the desired $CH_3S(O)CH_3$ concentration in the reaction gas. The concentration was continuously controlled at the outflow of the flow system by means of a proton transfer reaction mass spectrometer (Ionicon, PTR-MS 500) measuring the calibrated $(CH_3S(O)CH_3)H^+$ signal.

The initial $CH_3S(O)CH_3$ concentration of 4.2×10^{10} molecules cm^{-3}, significantly higher than atmospheric level, allowed to follow product formation from secondary OH chemistry under the chosen reaction conditions, i.e., the products arising from the OH + $CH_3S(O)OH$ reaction. The $CH_3S(O)OH$ conversion was below ~$(2 - 3) \times 10^8$ molecules cm^{-3}, that keeps the concentration of reactive intermediates low enough, i.e., below ~10^8 and mostly below 10^7 molecules cm^{-3}. Thus, unwanted bimolecular steps, such as $CH_3SO_2OO + RO_2$ (path **9** in Scheme 1**)** or any CH_3SO_3 reactions with peroxy species etc., were unimportant for the material balance even for bimolecular rate coefficients being close to the collision limit. This ensured the simplified data analysis as carried out. Relatively high concentrations of NO, higher than over the oceans, were used in order to elevate the CH_3SO_3 formation via path **8.** Consequently, the product concentrations of SO_3 and MSA were higher compared with low-NO conditions. The approach of determination of the temperature dependence of k_{11} is not affected by enhanced SO_3 concentrations using MSA formation via path **12** as the reference (assuming almost constant H-donor concentrations within a measurement series and an almost temperature-independent rate coefficient k_{12}).

All gas flows were set by means of calibrated gas flow controllers (MKS 1259/1179). The organic reactants and gases had the following purity: dimethyl sulfoxide (> 99.9 %, Aldrich), NO (498 ± 10 ppmV NO (99.5 %) in N_2 (99.999 %), Air Liquide) and NO_2 (≥ 99.5 %, Aldrich). Needed gas mixtures were prepared by means of a gas mixing unit using He as the dilution gas. Purified air was taken from a commercial PSA (Pressure Swing Adsorption) unit with further purification by a series of absorber units filled with hopcalite ($CuMnO_x$ catalyst), activated charcoal and different 4 Å and 10 Å molecular sieves.

Product formation was followed by means of a CI-APi-TOF (chemical ionization – atmospheric pressure interface – time-of-flight) mass spectrometer (Tofwerk AG, Airmodus) with a resolving power > 3000 Th/Th sampling from the center flow of the LFT with a rate of 10 L min^{-1} (STP). The ion-molecule reaction (IMR) took place at atmospheric pressure using a

Boulder-type inlet system.[4] As the reagent ions served iodide (I^-), bromide (Br^-), and nitrate (NO_3^-). Their precursors tert-butyl iodide, tert-butyl bromide and nitric acid, respectively, were added to a 35 L min^{-1} (STP) sheath flow of high-purity nitrogen forming the respective reagent ions after ionization with an ^{241}Am source.

$CH_3S(O)OH$, H_2SO_3 and $CH_3SO_2OONO_2$ were detected as the corresponding iodide adducts, (analyte)I^-, and SO_2 as $(SO_2)Br^-$ adduct. MSA and SO_3 were measured by means of nitrate ionization following the $CH_3SO_3^-$ and the $(CH_3SO_3H)NO_3^-$ signals or the SO_4^- and the $(SO_3)NO_3^-$ signals, respectively. Calibration factors needed for determination of product concentrations as well as their uncertainties were the same as described previously.[5] In the case of $CH_3SO_2OONO_2$, only lower limit concentrations with an uncertainty of a factor of two can be stated. Diffusion controlled wall loss for all products was considered using in each case $k_{loss} = 0.018\ s^{-1}$, see explanation in Berndt et al.[5].

2. Kinetic analysis

The rate law of CH_3SO_3 product formation, "CH_3SO_3-prod" meaning SO_3 and MSA, is given by:

$$\frac{d[CH_3SO_3 - prod.]}{dt} = k_8\,[NO] \times [CH_3SO_2OO] \#(S1)$$

The rate law for CH_3SO_2OO reads as follows:

$$\frac{d[CH_3SO_2OO]}{dt} = k_5\,[O_2] \times [CH_3SO_2] - k_{-5}\,[CH_3SO_2OO] - k_8\,[NO] \times [CH_3SO_2OO] \#(S2)$$

Steady-state approximation and the relationship $k_8\,[NO] \ll k_{-5}$ leads to:

$$[CH_3SO_2OO]_{ss} = \frac{k_5}{k_{-5}}\,[O_2] \times [CH_3SO_2] \#(S3)$$

Inserting Eq.S3 into Eq.S1 results in Eq.S4:

$$\frac{d[CH_3SO_3 - prod.]}{dt} = \frac{k_8 \times k_5}{k_{-5}}\,[NO] \times [O_2] \times [CH_3SO_2] \#(S4)$$

The rate law of SO_2 formation is given by:

$$\frac{d[SO_2]}{dt} = k_6\,[CH_3SO_2] \#(S5)$$

Eq.S4 and Eq.S5 result in Eq.S6 given that NO is not significantly consumed in the course of the reaction.

$$\frac{[CH_3SO_3 - prod.]}{[SO_2]} = \frac{[SO_3] + [MSA]}{[SO_2]} = \frac{k_8}{k_6}\frac{k_5}{k_{-5}}\,[O_2] \times [NO] \#(S6)$$

The measured ratio ([SO_3] + [MSA]) / [SO_2] as a function of NO allows a rough estimate of the equilibrium constant $K_5 = k_5 / k_{-5}$ within the proposed reaction scheme given in Scheme 1 as long as NO_2 reactions can be neglected. Rate coefficients k_6 and k_8 must be taken from the literature.

3. Reaction mechanism

This mechanism was used to calculate the HO_2 level and the HCHO production as well as the fraction of non-reacted CH_3SO_3 for the reaction time of 32 s. A comparison of measured $CH_3S(O)OH$ (MSIA) products with results from modeling confirmed the applicability of this mechanism, see Figure S3 in Berndt et al.[5].

Table S1: Reaction scheme describing the processes in the LFT. Rate coefficients at 295 K were taken from literature or have been estimated.

Reaction	**Rate coefficient (cm^3 $molecule^{-1}$ s^{-1} or s^{-1})**
IPN ($+O_2$) $\rightarrow$ NO + HO_2 + acetone	0.00039
NO + HO_2 $\rightarrow$ OH + NO_2	8.9×10^{-12} [6]
OH + HO_2 $\rightarrow$ H_2O + O_2	1.1×10^{-10} [6]
HO_2 + HO_2 $\rightarrow$ H_2O_2 + O_2	1.65×10^{-12} [6]
OH + NO $\rightarrow$ HNO_2	9.7×10^{-12} [6]
OH + NO_2 $\rightarrow$ HNO_3	1.2×10^{-11} [6]
OH + DMSO ($+O_2$) $\rightarrow$ MSIA + CH_3O_2	8.7×10^{-11} [7]
CH_3O_2 + HO_2 $\rightarrow$ ROOH + O_2	5.7×10^{-12} [6]
CH_3O_2 + NO ($+O_2$) $\rightarrow$ $0.9\times CH_2O$ + $0.9\times HO_2$ + $0.9\times NO_2$	7.7×10^{-12} [6]
OH + SO_2 ($+O_2$) $\rightarrow$ SO_3 + HO_2	8.9×10^{-13} [8]
OH + MSIA ($+O_2$) $\rightarrow$ $0.53\times H_2SO_3$ + $0.34\times SO_2$ + $0.87\times CH_3O_2$ + $0.13\times CH_3SO_3$	9.0×10^{-11} [7]
CH_3SO_3 ($+O_2$) $\rightarrow$ SO_3 + CH_3O_2	0.076 [2]
CH_3SO_3 + CH_2O $\rightarrow$ MSA + CHO	1.6×10^{-15} [9] #
OH $\rightarrow$ wall	0.053 §
HO_2 $\rightarrow$ wall	0.045 §
CH_3O_2 $\rightarrow$ wall	0.018 §
MSIA $\rightarrow$ wall	0.018 §
H_2SO_3 $\rightarrow$ wall	0.018 §
CH_3SO_3 $\rightarrow$ wall	0.018 §
SO_3 $\rightarrow$ wall	0.018 §

[#] this value is probably highly uncertain [§] diffusion-limited rate coefficient calculated for the LFT

4. Additional figures

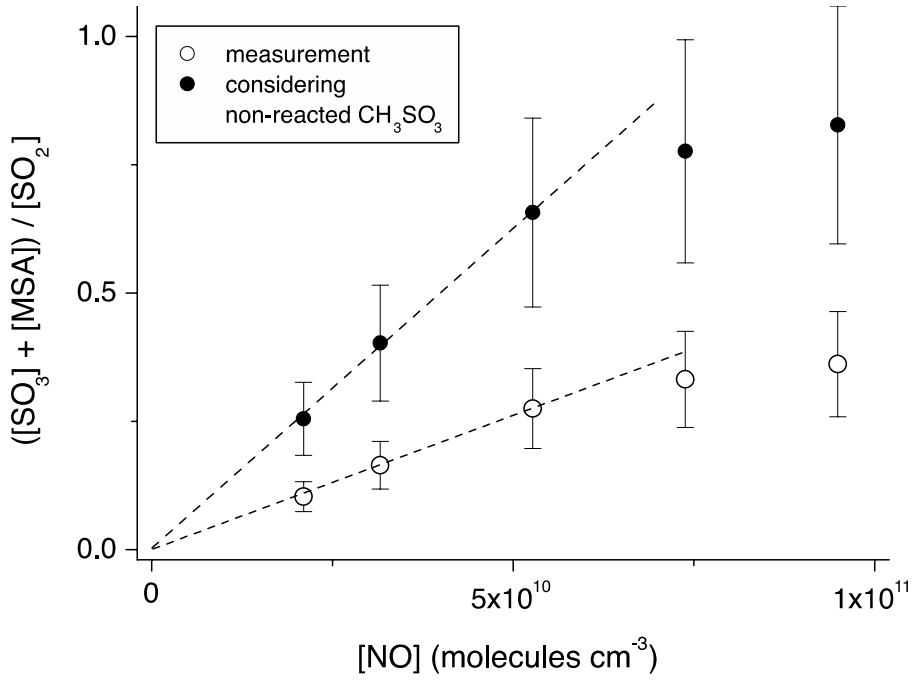

Fig.S1 Ratio of CH_3SO_3 products, SO_3 and MSA, and SO_2 as a function of NO concentration. The data were taken from the measurement series as depicted in Fig.1. Open circles represent the ratio of the measurement data. The amount of non-reacted CH_3SO_3, determined from modeling, is considered in the full circles. Only the first data points were taken for calculation of the slope $\Delta y / \Delta x = 5.2 \times 10^{-12}$ (open circle) and 1.25×10^{-11} cm^3 molecule^{-1} (full circle).

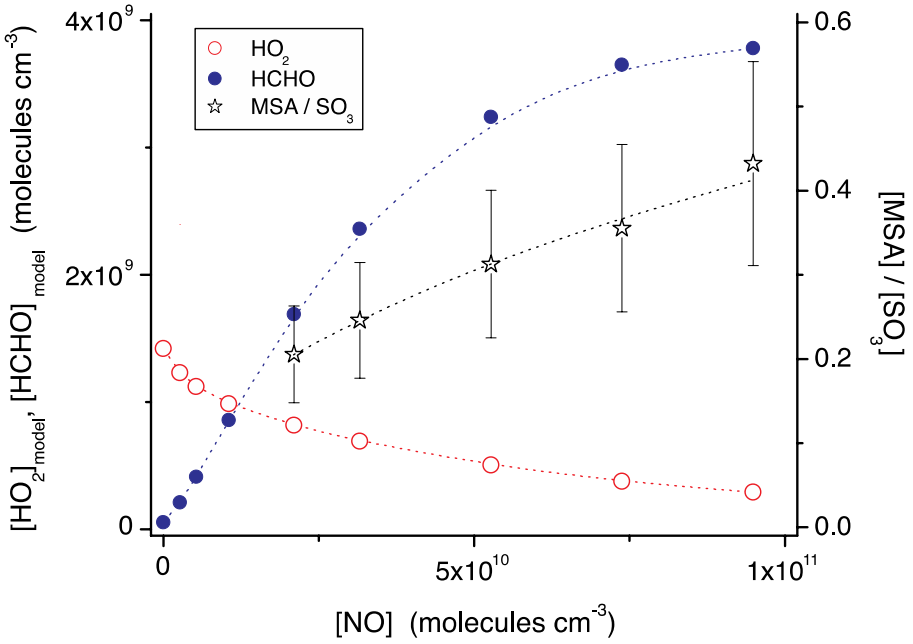

Fig.S2 Concentrations of HO_2 radicals and HCHO at the LFT outflow from modeling as well as the measured ratio [MSA] / [SO_3] as a function of NO concentration. The experimental data were taken from the measurement series as depicted in Fig.1.

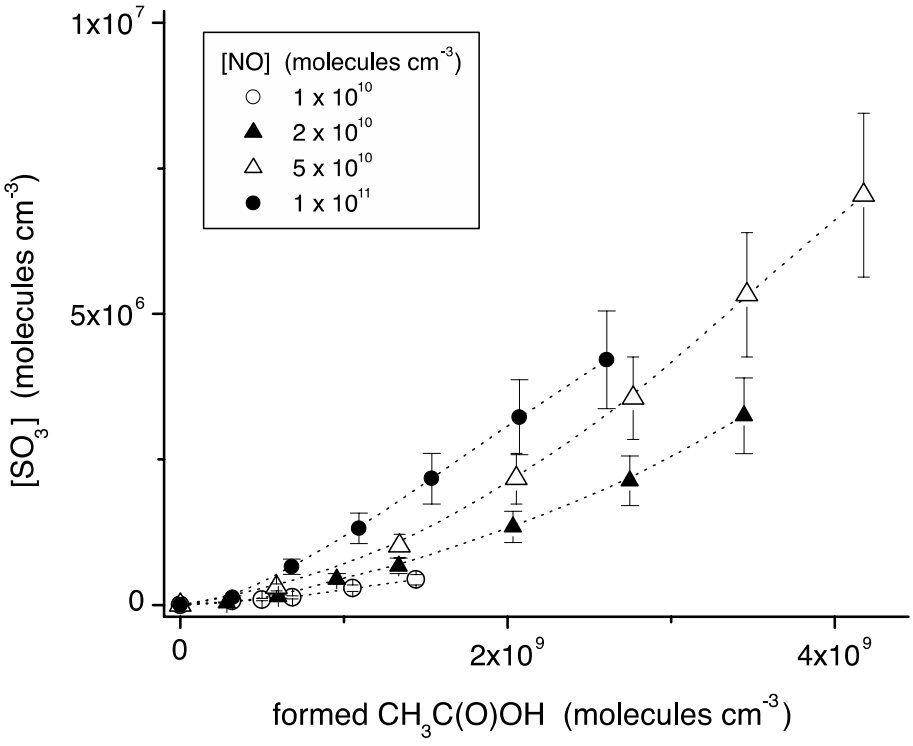

Fig.S3 Formed SO_3 (2^{nd} generation product) as a function of $CH_3C(O)OH$ (1^{st} generation product) for different NO levels from the reaction of OH radicals with $CH_3S(O)CH_3$. Increasing $CH_3S(O)CH_3$ conversion was achieved by rising IPN concentrations (rising OH radical concentrations) for constant $CH_3S(O)CH_3$ concentration of 4.2×10^{10} molecules cm^{-3}.

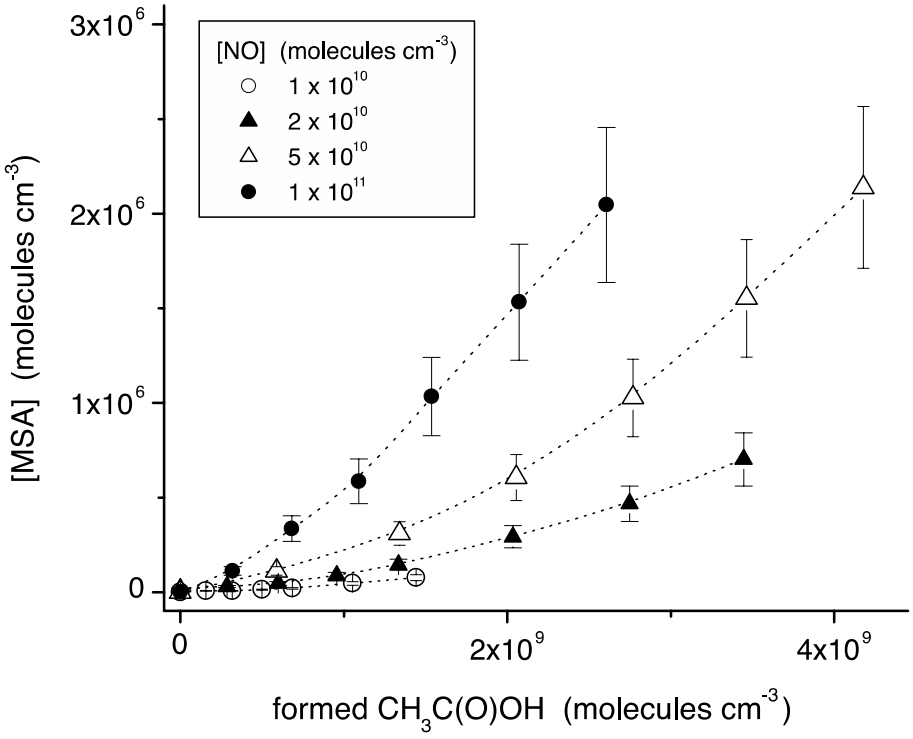

Fig.S4 MSA concentrations (2nd generation product) as a function of formed $CH_3C(O)OH$ (1st generation product) for different NO levels from the measurement series shown in Fig.S3.

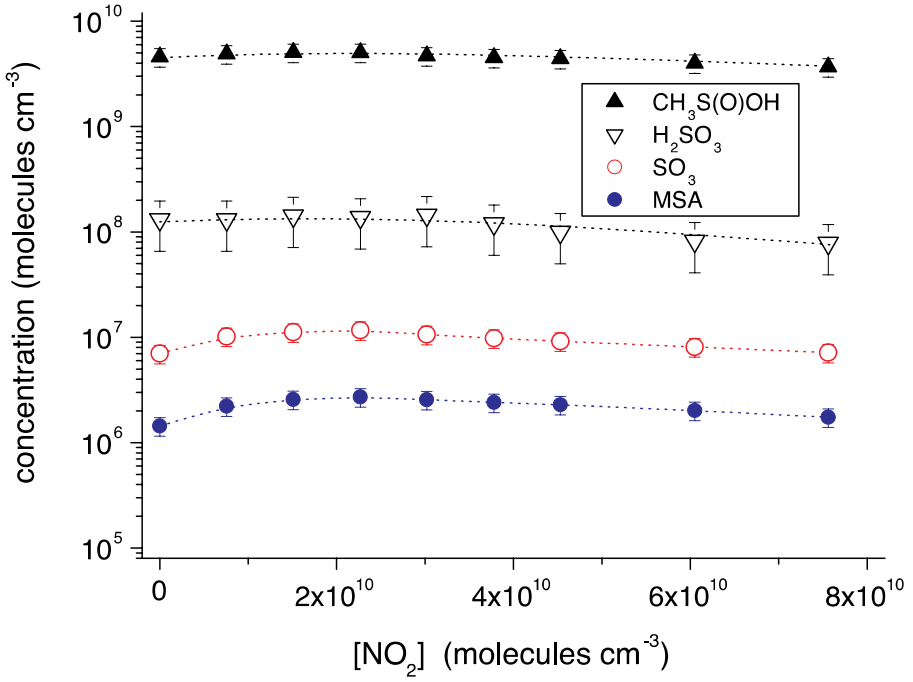

Fig.S5 Formation of $CH_3S(O)OH$, H_2SO_3, SO_3 and MSA (2nd generation products) from the OH + $CH_3S(O)CH_3$ reaction as a function of added NO_2, see also Fig.2. Error bars show the uncertainty derived from absolute calibrations. For H_2SO_3, the calibration factor of $CH_3S(O)OH$ was assumed with an uncertainty of ± 50 %. Reactant concentrations are given in the caption of Fig.2.

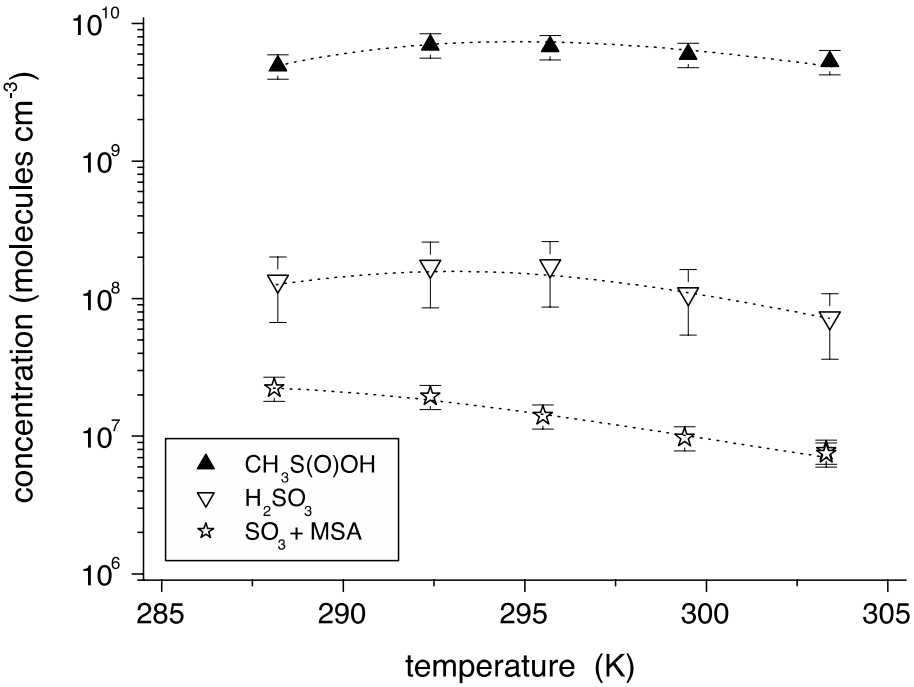

Fig.S6 Product concentrations of $CH_3S(O)OH$, H_2SO_3 and the sum of SO_3 and MSA as a function of temperature from the measurement series shown in Fig.3.

5. References

1. T. Berndt, H. Herrmann, M. Sipila, M. Kulmala, *J. Phys. Chem. A*, **2016**, *120*, 10150-10159.
2. T. Berndt, E. H. Hoffmann, A. Tilgner, F. Stratmann, H. Herrmann, *Nat. Commun.*, **2023**, *14*, 4849.
3. J. D. Raff, B. J. Finlayson-Pitts, *Environ. Sci. Technol.*, **2010**, *44*, 8150-8155.
4. F. L. Eisele, D. J. Tanner, *J. Geophys. Res.*, **1991**, *96*, 9295-9308.
5. T. Berndt, E. H. Hoffmann, A. Tilgner, H. Herrmann, *Angew. Chem. Int. Ed.*, **2024**, *63*, e202405572.
6. R. Atkinson, D. L. Bauch, R. A. Cox, R. F. Hampson, Jr., J. A. Kerr, J. Troe, *J. Phys. Chem. Ref. Data*, **1992**, *21*, 1125-1568.
7. I. Barnes, J. Hjorth, N. Mihalopoulos, *Chem. Rev.* **2006**, *106*, 940-975.
8. R. Atkinson, D. L. Baulch, R. A. Cox, J. N. Crowley, R. F. Hampson, R. G. Hynes, M. E. Jenkin, M. J. Rossi, J. Troe, *Atmos. Chem. Phys.* **2004**, *4*, 1461-2004.
9. F. Yin, D. Grosjean, J. H. Seinfeld, *J. Atmos. Chem.*, **1990**, *11*, 309-364.